

6.3 EFFECT OF HORIZONTAL SURFACE TEMPERATURE HETEROGENEITY ON TURBULENT MIXING IN THE STABLY STRATIFIED ATMOSPHERIC BOUNDARY LAYER

Dmitrii V. Mironov^{1*} and Peter P. Sullivan²

¹ German Weather Service, Offenbach am Main, Germany

² National Center for Atmospheric Research, Boulder, CO, USA

1. INTRODUCTION

Representation of stably-stratified boundary-layer turbulence in numerical models of atmospheric circulation is one of the key unresolved issues that slows down progress in climate modeling, numerical weather prediction, and related applications. Turbulence in a stably stratified boundary layer (SBL) is weak and often intermittent in space and time. It responds to various effects, for example, internal gravity waves, cold air meandering, and horizontal inhomogeneity of the underlying surface. Current SBL models (parameterization schemes) do not include these important effects in a physically meaningful way.

The majority of SBL turbulence models are based on truncated budget equations for the second-order moments of fluctuating fields. In spite of their fundamental importance (see a discussion in Mironov, 2009), the second-moment budgets in the SBL have not been systematically analyzed so far. In most large-eddy simulation (LES) and direct numerical simulation (DNS) studies performed to date, the emphasis is on the turbulence kinetic energy (TKE) budget (e.g. Coleman et al., 1992; Brown et al., 1994; Kosović and Curry, 2000; Saiki et al., 2000; Jiménez and Cuxart, 2005; van Dop and Axelsen, 2007; Taylor and Sarkar, 2008). Very few attempts have been made to analyze other second-moment budgets, such as the budget of temperature variance (e.g. Mason and Derbyshire, 1990) and of Reynolds stress and scalar flux (e.g. André, 1995). It should also be noted that the LES-based second-moment budgets are often estimated on the basis of resolved-scale fields only. However, the sub-grid scale (SGS) contributions may be substantial, particularly in the SBL, and should be retained in order to close the second-moment budgets to a good order. In the present study, the budgets of TKE, of the potential temperature variance, and of the vertical component of the potential temperature flux are considered using a data set generated by LES.

Another important aspect of the SBL that is not yet satisfactorily understood is how surface heterogeneity, e.g. with respect to the temperature, modifies the structure and the transport properties of the SBL turbulence. Stoll and Porté-Agel (2009) performed LES of SBL over a temperature-homogeneous surface and over a temperature-heterogeneous surface where spanwise homogeneous surface temperature patches alternate between two temperature values but the horizontal-mean surface temperature is the same as in their homogeneous runs. They found, among other things, that the heterogeneous SBL is more turbulent and is better mixed with respect to mean potential temperature. We attempt to explain the enhanced vertical mixing in the SBL over temperature-heterogeneous surface through a comparative analysis of the second-moment budgets in homogeneous and heterogeneous SBLs.

In what follows, we use standard notation where t is time, x_i are the right-hand Cartesian co-ordinates, u_i are the velocity components, θ is the potential temperature (for the sake of brevity, it will also be referred to as simply “temperature”), p is the kinematic pressure (deviation of pressure from the hydrostatically balanced pressure divided by the reference density ρ_r), $\beta_i = -g_i/\theta_r$ is the buoyancy parameter, g_i is the acceleration due to gravity, θ_r is the reference value of temperature, and f is the Coriolis parameter. The Einstein summation convention for repeated indices is adopted. An overbar ($\overline{\quad}$) denotes a resolved-scale (filtered) variable computed by a large-eddy model. The angle brackets $\langle(\quad)\rangle$ denote a horizontal mean, and a double prime $(\quad)''$ denotes a fluctuation about a horizontal mean.

2. LES DATA SET

The LES code used in the present study is described in detail in Moeng (1984), Moeng and Wyngaard (1988), Sullivan et al. (1994, 1996), and Sullivan and Patton (2008). The Boussinesq approximation is used which is a fairly accurate approximation for the lower troposphere. In our simplified configuration, potential temperature is the only thermodynamic variable that affects the distribu-

*Corresponding author address: Dmitrii V. Mironov, Deutscher Wetterdienst, FE14, Frankfurter Str. 135, D-63067 Offenbach am Main, Germany; e-mail: dmitrii.mironov@dwd.de

tion of buoyancy. The x_3 axis is aligned with the vector of gravity and is directed upwards. The buoyancy parameter $\beta_3 = -g_3/\theta_r$ is constant, where $g_3 = -9.81 \text{ m}\cdot\text{s}^{-1}$ and $\theta_r = 265 \text{ K}$.

One SBL flow with the temperature-homogeneous underlying surface, referred to as case HOM, and one flow with the temperature-heterogeneous surface, referred to as case HET, are generated. In both simulations, the number of grid points is 200, 200, and 192 in the streamwise x_1 , spanwise x_2 , and vertical x_3 directions, respectively, and the numerical domain size is 400 m in all directions. The flows are driven by a constant streamwise geostrophic wind $U_g = 8.0 \text{ m}\cdot\text{s}^{-1}$; the spanwise geostrophic wind V_g is zero. The Coriolis parameter is $f = 1.39 \cdot 10^{-4} \text{ s}^{-1}$, and the surface roughness length for both wind and temperature is $z_0 = 10^{-1} \text{ m}$.

In both simulated cases, periodic boundary conditions are applied in the x_1 and x_2 horizontal directions. At the upper boundary of the numerical domain, zero SGS TKE, free-slip for the horizontal velocity components, the potential temperature lapse rate $\Gamma_\theta = 10^{-2} \text{ K}\cdot\text{m}^{-1}$, and the radiative boundary conditions that allow internal gravity waves to leave the system are applied. At the underlying surface, velocities are zero, and the vertical fluxes of horizontal momentum and of heat (temperature) are evaluated from surface layer similarity. The Monin-Obukhov surface-layer flux-profile relationships are applied locally, i.e. point-by-point in the LES. The surface fluxes for each model grid box are computed using the surface temperature and the temperature and velocity at the first model level above the ground.

The time varying surface temperature is determined by a specified surface cooling rate. In the homogeneous case, a constant cooling rate $R_c = -0.375 \text{ K}\cdot\text{hr}^{-1}$ is applied over the first 8 hours of the simulations. In the heterogeneous case, the cooling rate is constant in the spanwise direction and varies sinusoidally in the streamwise direction as $(\partial\bar{\theta}/\partial t)_{sfc} = R_c [1 + \sin(2\pi x_1/L_1)]$, where L_1 is the domain size in the x_1 direction. The horizontal-mean surface temperature is the same as in the homogeneous case. Eight hours of cooling lead to a surface temperature difference of 6 K between the warm and the cold stripes. Following this initial period, both simulations are continued, using a constant cooling rate R_c . The set-up of our simulation is broadly similar to that of Stoll and Porté-Agel (2009) differing in the magnitude of the surface cooling rate and the shape of the surface-temperature heterogeneity patterns (a series of spanwise homogeneous surface temperature patches that alternate between two temperature values in the simulations of Stoll and Porté-Agel versus a sinusoidal variation of the surface temperature in our simulations).

The initial temperature profile has a two-layer structure. A layer of depth $h_i = 100 \text{ m}$ and depth-constant

temperature $\bar{\theta} = \theta_r$ is capped by a stratified layer where the temperature increases linearly at a rate Γ_θ . The initial velocity components \bar{u}_2 and \bar{u}_3 in the spanwise and vertical direction, respectively, are zero throughout the domain. The initial streamwise velocity component \bar{u}_1 is set equal to U_g . To facilitate the growth of turbulence, small random disturbances are added to the initial temperature and velocity fields in the lower part of the domain ($x_3 < h_i$), and the SGS TKE there is set to a small value.

In order to obtain approximations to ensemble-mean quantities, the LES data are averaged over horizontal planes and the resulting profiles are then averaged over several thousand time steps. The number of samples varies between the two cases but the sampling time covers the last 1.75 hours of simulations. It should be noted that the LES averages (presumably) tend to the true ensemble-mean quantities as the resolution is increased.

3. MEAN FIELDS AND SECOND-ORDER MOMENTS

Vertical profiles of the streamwise $U = \langle \bar{u} \rangle$ and the spanwise $V = \langle \bar{v} \rangle$ mean wind components and of mean temperature $\Theta = \langle \bar{\theta} \rangle$ are shown in Fig. 1. A comparison of cases HOM and HET suggests that in the latter the SBL is deeper. The components of mean wind are quite similar in shape in both cases (except for $\langle \bar{v} \rangle$ near the boundary layer top), whereas the mean temperature profiles are essentially different. The SBL over a temperature-heterogeneous surface is much better mixed with respect to $\langle \bar{\theta} \rangle$. The results shown in Fig. 1 confirm previous findings of Stoll and Porté-Agel (2009).

Figure 2 shows vertical profiles of turbulence kinetic energy, $\text{TKE} = \langle \bar{u}_i'^2 \rangle + \langle e \rangle$, temperature variance, $\text{TT} = \langle \bar{\theta}''^2 \rangle + \langle \vartheta \rangle$, and vertical temperature flux, $U_3\text{T} = \langle \bar{u}_3''\bar{\theta}'' \rangle + \langle \tau_{3\theta} \rangle$. The second-order moments are estimated with due regard for the SGS contributions. The SGS TKE e and (the vertical component of) the SGS temperature flux $\tau_{3\theta}$ are computed by the SGS model. The SGS temperature variance ϑ , which is not computed by the SGS model, is estimated as $\vartheta = 5\tau_{i\theta}^2/e$, where the numerical value of the coefficient follows from the consideration of the inertial sub-range temperature spectrum (Moeng and Wyngaard, 1988).

The TKE in the heterogeneous case is larger and the magnitude of the downward temperature (heat) flux is reduced over most of the boundary layer. The temperature variance reveals an even more striking difference between HOM and HET. In the heterogeneous case, it has a distinct maximum near the SBL top, apparently due to an increased mean temperature gradient and hence an increased temperature-variance production. The most

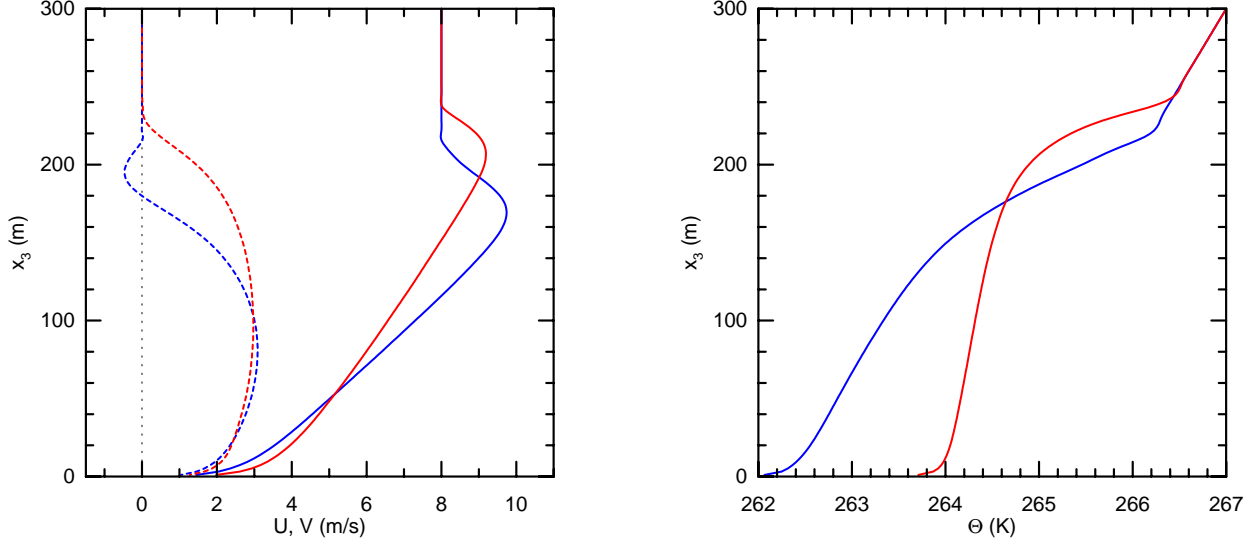


Figure 1: Streamwise (solid curves) and spanwise (dashed curves) components of mean wind (left panel) and mean temperature (right panel) from simulations HOM (blue) and HET (red).

pronounced difference between HOM and HET is close to the surface where the temperature variance is much larger in the heterogeneous case. This increase in the temperature variance helps explain the reduced magnitude of the downward temperature flux and more vigorous mixing in the heterogeneous SBL. The issue is discussed below in more detail in the context of comparative analysis of the second-moment budgets.

4. SECOND-ORDER MOMENT BUDGETS

First, we briefly explain how approximations to the ensemble-mean budget equations for the second-order moments are obtained from numerical data generated with an LES. It should be emphasized that the second-moment budgets derived from LES are not the same as the ensemble-mean budgets. The relation between the two sets of budget equations is not entirely straightforward, and the approach used by various authors is not always made clear.

Consider the budget of the temperature variance. We “forget” for a moment that the averaging denoted by angle brackets is the averaging over the horizontal that makes a number of terms in the second-moment budgets disappear. The temperature-variance budget equation is first presented in its full three-dimensional form. Then, it is simplified by taking the properties of the horizontal averaging into account.

The budget equation for the resolved-scale temperature variance $\langle \bar{\theta}''^2 \rangle$ is obtained from the filtered tem-

perature equation in a usual way. Subtracting from the transport equation for $\bar{\theta}$ its horizontal mean yields the equation for $\bar{\theta}''$. Multiplying that equation by $\bar{\theta}''$ and averaging the result yields the equation for $\langle \bar{\theta}''^2 \rangle$. It reads

$$\frac{1}{2} \left(\frac{\partial}{\partial t} + \langle \bar{u}_i \rangle \frac{\partial}{\partial x_i} \right) \langle \bar{\theta}''^2 \rangle =$$

$$- \langle \bar{u}_i'' \bar{\theta}'' \rangle \frac{\partial \langle \bar{\theta} \rangle}{\partial x_i} - \frac{1}{2} \frac{\partial}{\partial x_i} \langle \bar{u}_i'' \bar{\theta}''^2 \rangle - \langle \bar{\theta}'' \frac{\partial \tau_{i\theta}''}{\partial x_i} \rangle, \quad (1)$$

where $\tau_{i\theta} = \overline{u_i \theta} - \bar{u}_i \bar{\theta}$ is the SGS temperature flux. We use the Lilly (1967) notation with no primes to emphasize that the filter operator used to derive the governing equations of a large-eddy model should not necessarily satisfy the Reynolds averaging assumption. The first two terms on the right-hand side (r.h.s.) of Eq. (1) represent the effects of the mean-gradient production-destruction and of the turbulent transport of the resolved-scale temperature variance, respectively. The physical meaning of the last term on the r.h.s. is discussed below. Recall that the filtered equations used by a high Reynolds number LES do not contain molecular terms. As a result, the equations for the resolved-scale second-order moments do not contain molecular destruction terms, these are small and are safely neglected.

The averaged budget equation for the SGS temperature variance $\vartheta = \bar{\theta}^2 - \bar{\theta}^2$ reads (see Lilly, 1967, and Deardorff, 1973, where the transport equations for the

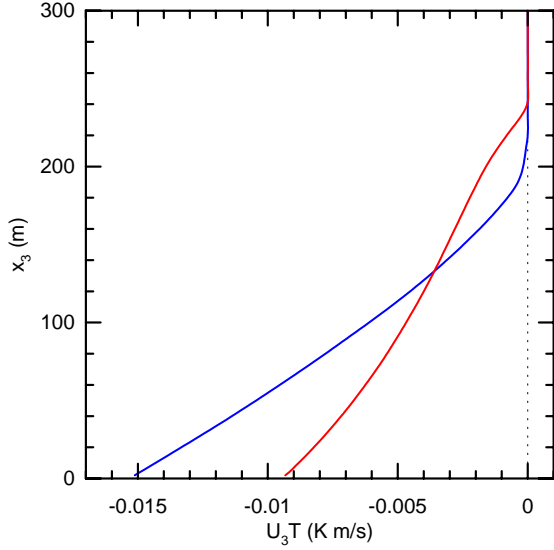
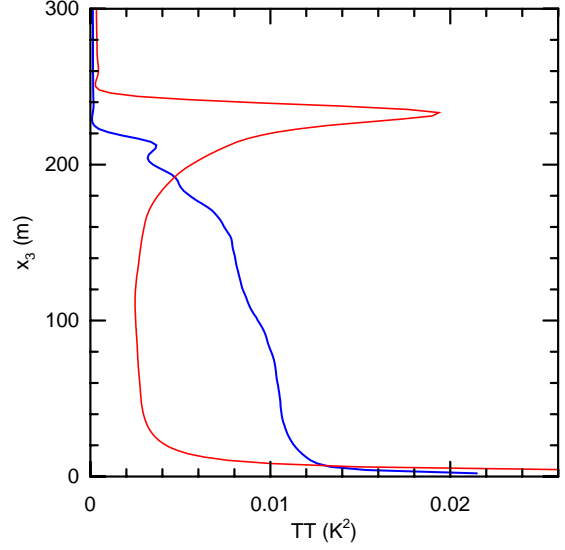
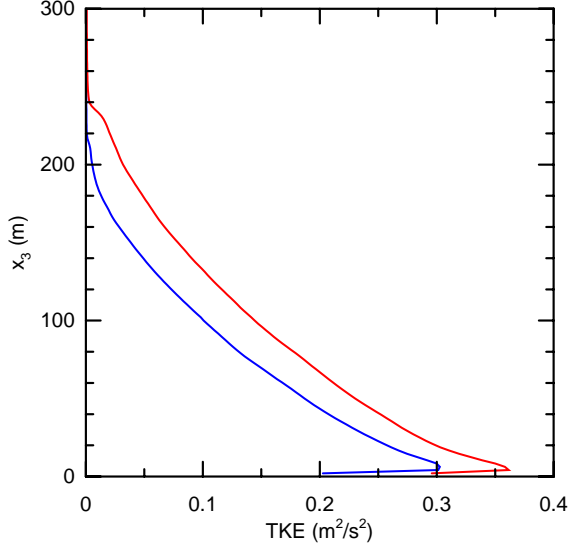


Figure 2: TKE, temperature variance TT, and vertical temperature flux U_3T from simulations HOM (blue curves) and HET (red curves).

SGS quantities are considered in detail)

$$\frac{1}{2} \left(\frac{\partial}{\partial t} + \langle \bar{u}_i \rangle \frac{\partial}{\partial x_i} \right) \langle \vartheta \rangle = - \left\langle \tau_{i\vartheta} \frac{\partial \bar{\theta}}{\partial x_i} \right\rangle - \frac{1}{2} \frac{\partial}{\partial x_i} \left(\langle \bar{u}_i'' \vartheta'' \rangle + \langle \mathcal{I}_{i\vartheta} \rangle \right) - \langle \varepsilon_\theta \rangle, \quad (2)$$

where $\mathcal{I}_{i\vartheta} = \overline{u_i \theta^2} - \bar{u}_i \bar{\theta}^2 + 2 \left(\overline{u_i \theta^2} - \bar{u}_i \bar{\theta} \bar{\theta} \right)$ is the SGS triple correlation (SGS flux of ϑ), and ε_θ is the temperature-variance dissipation rate.

The first term on the r.h.s. of Eq. (2) is re-arranged to give

$$- \left\langle \tau_{i\vartheta} \frac{\partial \bar{\theta}}{\partial x_i} \right\rangle =$$

$$- \langle \tau_{i\vartheta} \rangle \frac{\partial \langle \bar{\theta} \rangle}{\partial x_i} - \frac{\partial}{\partial x_i} \langle \bar{\theta}'' \tau_{i\vartheta}'' \rangle + \left\langle \bar{\theta}'' \frac{\partial \tau_{i\vartheta}''}{\partial x_i} \right\rangle. \quad (3)$$

Substituting (3) into (2), we obtain

$$\frac{1}{2} \left(\frac{\partial}{\partial t} + \langle \bar{u}_i \rangle \frac{\partial}{\partial x_i} \right) \langle \vartheta \rangle = - \langle \tau_{i\vartheta} \rangle \frac{\partial \langle \bar{\theta} \rangle}{\partial x_i} - \frac{1}{2} \frac{\partial}{\partial x_i} \left(\langle \bar{u}_i'' \vartheta'' \rangle + 2 \langle \bar{\theta}'' \tau_{i\vartheta}'' \rangle + \langle \mathcal{I}_{i\vartheta} \rangle \right) - \langle \varepsilon_\theta \rangle + \left\langle \bar{\theta}'' \frac{\partial \tau_{i\vartheta}''}{\partial x_i} \right\rangle, \quad (4)$$

where the first and the second terms on the r.h.s. of Eq. (4) represent the mean-gradient production-destruction and the transport of the SGS temperature

variance, respectively. These terms are similar in nature to the the first and the second terms, respectively, on the r.h.s. of Eq. (1) for the resolved-scale temperature variance. The last term on the r.h.s. of Eq. (4) is equal in magnitude but opposite in sign to the last term on the r.h.s. of Eq. (1). It may be referred to as the scale interaction term that describes the transfer of the temperature variance between the resolved and the sub-grid scales. Clearly, this term disappears if the total, i.e. resolved + SGS, temperature variance is considered.

Adding Eqs. (1) and (4) yields the budget equation for the total temperature variance $\langle \bar{\theta}''^2 \rangle + \langle \vartheta \rangle$. It reads

$$\begin{aligned} \frac{1}{2} \left(\frac{\partial}{\partial t} + \langle \bar{u}_k \rangle \frac{\partial}{\partial x_k} \right) \left(\langle \bar{\theta}''^2 \rangle + \langle \vartheta \rangle \right) = \\ - \left(\langle \bar{u}_i'' \bar{\theta}'' \rangle + \langle \tau_{i\theta} \rangle \right) \frac{\partial \langle \bar{\theta} \rangle}{\partial x_i} - \langle \epsilon_\theta \rangle \\ - \frac{1}{2} \frac{\partial}{\partial x_i} \left[\langle \bar{u}_i'' \bar{\theta}''^2 \rangle + \langle \bar{u}_i'' \vartheta'' \rangle + 2 \langle \bar{\theta}'' \tau_{i\theta}'' \rangle + \langle \mathcal{T}_{i\vartheta} \rangle \right]. \quad (5) \end{aligned}$$

The terms on the r.h.s. of Eq. (5) are treated as approximations to the mean-gradient production-destruction, the dissipation, and the transport terms in the ensemble-mean temperature-variance budget equation. It should always be remembered, however, that we deal with the LES estimates that (presumably) tend to the ensemble-mean budgets as the resolution is increased.

With due regard for the periodic boundary conditions in x_1 and x_2 horizontal directions and zero horizontal-mean vertical velocity $\langle \bar{u}_3 \rangle$, Eq. (5) is somewhat simplified to give the following temperature-variance budget equation:

$$\begin{aligned} \frac{1}{2} \frac{\partial}{\partial t} \left(\langle \bar{\theta}''^2 \rangle + \langle \vartheta \rangle \right) = - \left(\langle \bar{u}_3'' \bar{\theta}'' \rangle + \langle \tau_{3\theta} \rangle \right) \frac{\partial \langle \bar{\theta} \rangle}{\partial x_3} - \langle \epsilon_\theta \rangle \\ - \frac{1}{2} \frac{\partial}{\partial x_3} \left[\langle \bar{u}_3'' \bar{\theta}''^2 \rangle + \langle \bar{u}_3'' \vartheta'' \rangle + 2 \langle \bar{\theta}'' \tau_{3\theta}'' \rangle + \langle \mathcal{T}_{3\vartheta} \rangle \right]. \quad (6) \end{aligned}$$

An approximation to the temperature-variance dissipation rate is computed as $\langle \epsilon_\theta \rangle = \langle K_H (\partial \bar{\theta} / \partial x_i)^2 \rangle$, where K_H is the SGS temperature conductivity. The SGS triple correlation term $\langle \mathcal{T}_{3\vartheta} \rangle$ cannot be estimated from our LES data and is treated as the budget imbalance. It is presumably small.

The budget equations for the TKE and for the potential temperature flux are derived in a similar way. With due regard for the periodic boundary conditions in horizontal directions, they read

$$\frac{\partial}{\partial t} \left(\frac{1}{2} \langle \bar{u}_i''^2 \rangle + \langle e \rangle \right) =$$

$$\begin{aligned} - \left[\left(\langle \bar{u}_1'' \bar{u}_3'' \rangle + \langle \tau_{13} \rangle \right) \frac{\partial \langle \bar{u}_1 \rangle}{\partial x_3} + \left(\langle \bar{u}_2'' \bar{u}_3'' \rangle + \langle \tau_{23} \rangle \right) \frac{\partial \langle \bar{u}_2 \rangle}{\partial x_3} \right] \\ + \beta_3 \left(\langle \bar{u}_3'' \bar{\theta}'' \rangle + \langle \tau_{3\theta} \rangle \right) - \langle \epsilon \rangle \\ - \frac{\partial}{\partial x_3} \left(\frac{1}{2} \langle \bar{u}_3'' \bar{u}_i''^2 \rangle + \langle \bar{u}_3'' e'' \rangle + \langle \bar{u}_i'' \tau_{i3}'' \rangle + \langle \bar{u}_3'' \bar{p}'' \rangle \right. \\ \left. + \frac{1}{2} \langle \mathcal{T}_{3ii} \rangle + \langle \bar{u}_3 \bar{p} - \bar{u}_3 \bar{p} \rangle \right), \quad (7) \end{aligned}$$

$$\begin{aligned} \frac{\partial}{\partial t} \left(\langle \bar{u}_3'' \bar{\theta}'' \rangle + \langle \tau_{3\theta} \rangle \right) = - \left(\langle \bar{u}_3''^2 \rangle + \langle \tau_{33} \rangle \right) \frac{\partial \langle \bar{\theta} \rangle}{\partial x_3} \\ + \beta_3 \left(\langle \bar{\theta}''^2 \rangle + \langle \vartheta \rangle \right) - \left(\langle \bar{\theta}'' \frac{\partial \bar{p}''}{\partial x_3} \rangle + \left\langle \bar{\theta} \frac{\partial \bar{p}}{\partial x_3} - \bar{\theta} \frac{\partial \bar{p}}{\partial x_3} \right\rangle \right) \\ - \frac{\partial}{\partial x_3} \left(\langle \bar{u}_3'' \bar{\theta}''^2 \rangle + 2 \langle \bar{u}_3'' \tau_{3\theta}'' \rangle + \langle \bar{\theta}'' \tau_{33}'' \rangle + \langle \mathcal{T}_{33\theta} \rangle \right). \quad (8) \end{aligned}$$

Here, $\tau_{ij} = \bar{u}_i \bar{u}_j - \bar{u}_i \bar{u}_j$ is the SGS Reynolds stress, $e = \tau_{ii}/2$ is the SGS TKE, and $\mathcal{T}_{3ii} = \bar{u}_3 \bar{u}_i^2 - \bar{u}_3 \bar{u}_i^2 + 2(\bar{u}_3 \bar{u}_i^2 - \bar{u}_i \bar{u}_i \bar{u}_3)$ and $\mathcal{T}_{33\theta} = \bar{u}_3^2 \bar{\theta} - \bar{u}_3^2 \bar{\theta} + 2(\bar{u}_3 \bar{\theta} - \bar{u}_3 \bar{u}_3 \bar{\theta})$ are the third-order SGS transport terms (SGS fluxes of the SGS TKE and of the SGS temperature flux). An estimate of the TKE dissipation rate $\langle \epsilon \rangle$ stems from the SGS TKE equation carried by the large-eddy model. An approximation to the SGS pressure-gradient-temperature covariance is computed as $\langle \bar{\theta} \partial \bar{p} / \partial x_3 - \bar{\theta} \partial \bar{p} / \partial x_3 \rangle = - \langle \tau_{i\theta} \partial \bar{u}_3 / \partial x_i \rangle - \langle \tau_{3i} \partial \bar{\theta} / \partial x_i \rangle + \beta_3 \langle \vartheta \rangle$ (see Mironov et al., 2000, and Mironov, 2001, for details). Results from previous studies suggest (Khanna, 1998; Mironov et al., 2000; Mironov, 2001) that the SGS pressure term should be added to the resolved-scale pressure term in order to close the temperature-flux budget to a good order.

Notice that the third-order SGS transport terms $\mathcal{T}_{3\vartheta}$ in Eq. (6) and $\mathcal{T}_{33\theta}$ in Eq. (8) cannot be estimated from our LES data as these terms are not computed within the SGS model. The third-order SGS transport term in the TKE equation (7) can be estimated. However, it is the entire transport term, $\frac{1}{2} \mathcal{T}_{jii} + \bar{u}_j \bar{p} - \bar{u}_j \bar{p}$, that is parameterised through the down-gradient diffusion approximation in the SGS TKE equation. Hence, it is impossible to discriminate between the third-order transport and the pressure transport of the SGS TKE by the SGS fluctuating motions.

The second-moment budgets from simulations HOM and HET are shown in Figs. 3–5. The budget imbalance

is computed as the sum of terms on the r.h.s. of Eqs. (6)–(8). In all budgets, the imbalance is small as compared to the leading-order terms but is not entirely negligible. Notice, however, that turbulence in our SBL flows is never in a perfectly steady state. Continuous decrease of the surface temperature causes continuous adjustment of the SBL turbulence structure to changing static stability. Then, the tendencies of the TKE, of the temperature flux and of the temperature variance are likely the major contributions to the imbalance of the respective budget, whereas other contributions, e.g. due to sampling errors, are small.

The TKE budgets from simulations HOM and HET are shown in Fig. 3. In both cases, the budget is dominated by the mean velocity shear and the dissipation terms. The turbulent transport term is small over most of the SBL, except in the near vicinity of the surface where it is an energy sink. The major difference between the two budgets is in the buoyancy flux. In the heterogeneous case, its magnitude is substantially reduced.

The budget of the vertical temperature flux, Fig. 4, is maintained by the mean temperature gradient term, the buoyancy term, and the pressure-gradient–temperature covariance. The turbulent transport term is small in both cases. The major difference between HOM and HET is in the buoyancy term. In the homogeneous case, it has a pronounced maximum near the SBL top and, most notably, it is very large near the surface.

The largest difference between HOM and HET is exhibited by the temperature-variance budget, Fig. 5. In the homogeneous case, the vertical flux of temperature variance is zero at the surface and at the SBL top. Hence, the turbulent transport term, i.e. the divergence of the above third-order flux, acts to redistribute the temperature variance in the vertical. It integrates to zero over the entire SBL. In the heterogeneous case, the transport term does not integrate to zero and is a net gain for the temperature variance. This is only possible if the flux of temperature variance is non-zero at the surface.

The expression for the vertical flux of temperature variance in Eq. (6) reads

$$\langle \bar{u}_3'' \bar{\theta}''^2 \rangle + \langle \bar{u}_3'' v'' \rangle + 2 \langle \bar{\theta}'' \tau_{3\theta}'' \rangle + \langle \mathcal{I}_{3\theta} \rangle. \quad (9)$$

The last term in Eq. (9) cannot be estimated from our LES but is most likely small. The first two terms are zero at the surface due to zero resolved vertical velocity \bar{u}_3 . The third term is zero in HOM since the surface is homogeneous with respect to the temperature $\bar{\theta}$. This is not the case in HET where the surface temperature varies in the streamwise direction. Surface temperature variations modify local stability conditions thus modulating the surface temperature flux, so that $\bar{\theta}$ and $\tau_{3\theta}$ are correlated. Positive fluctuations of temperature about its

horizontal mean, $\bar{\theta}'' > 0$, reduces local temperature gradient, leading to a reduced magnitude of the downward (negative) temperature flux, i.e. $\tau_{3\theta}'' > 0$. And vice versa, negative temperature fluctuations, $\bar{\theta}'' < 0$, increase local temperature gradient, leading to $\tau_{3\theta}'' < 0$. Then, $\bar{\theta}$ and $\tau_{3\theta}$ appear to be positively correlated leading to a positive temperature-variance flux at the surface. It should be stressed that the result cannot be obtained if the third-order moment (flux of temperature variance) is estimated on the basis of resolved-scale fields only, i.e. keeping only the first term in Eq. (9).

The above analysis suggests the following qualitative explanation of enhanced vertical mixing in the SBL over a temperature-heterogeneous surface. Due to heterogeneity, the temperature variance near the surface strongly increases. The temperature variance (multiplied by the buoyancy parameter) enters the temperature flux budget, Eq. (8), as the buoyancy production term. As it acts to generate a positive (upward) temperature flux, an increased temperature variance partially compensates the mean gradient term that acts to generate a negative (downward) temperature flux. As a result, the downward temperature flux is reduced in magnitude. Since in a quasi-steady SBL the vertical temperature flux is nearly linear (see Fig. 2), a reduction occurs not only near the surface but also over most of the SBL. In stable stratification, the buoyancy flux (temperature flux times the buoyancy parameter) is the sink term in the TKE budget, Eq. (7). A reduced magnitude of the buoyancy flux assumes that less energy is spent to work against the gravity, leading to an increased TKE (Fig. 2) and more vigorous mixing in the heterogeneous SBL as compared to its homogeneous counterpart.

5. DISCUSSION

The above analysis suggests a key role of the temperature variance in turbulent mixing in a horizontally heterogeneous SBL. In order to incorporate the effect of surface temperature heterogeneity, SBL turbulence models (parameterization schemes) should account for an increased temperature variance near the surface and a non-zero temperature-variance flux. Turbulence closures applied to the entire SBL should account for the above effect in a physically meaningful way (e.g. through the use of temperature-variance transport equation with a physically sound parameterization of the third-order moment), but also the surface-layer flux-profile relationships should be modified accordingly. The task is notoriously difficult, and the authors admit they have no solution to this problem. There seems to be a way out, however, which is perhaps less attractive than improved flux-profile relationships but is quite reasonable from the practical standpoint. The idea is to use a tile approach,

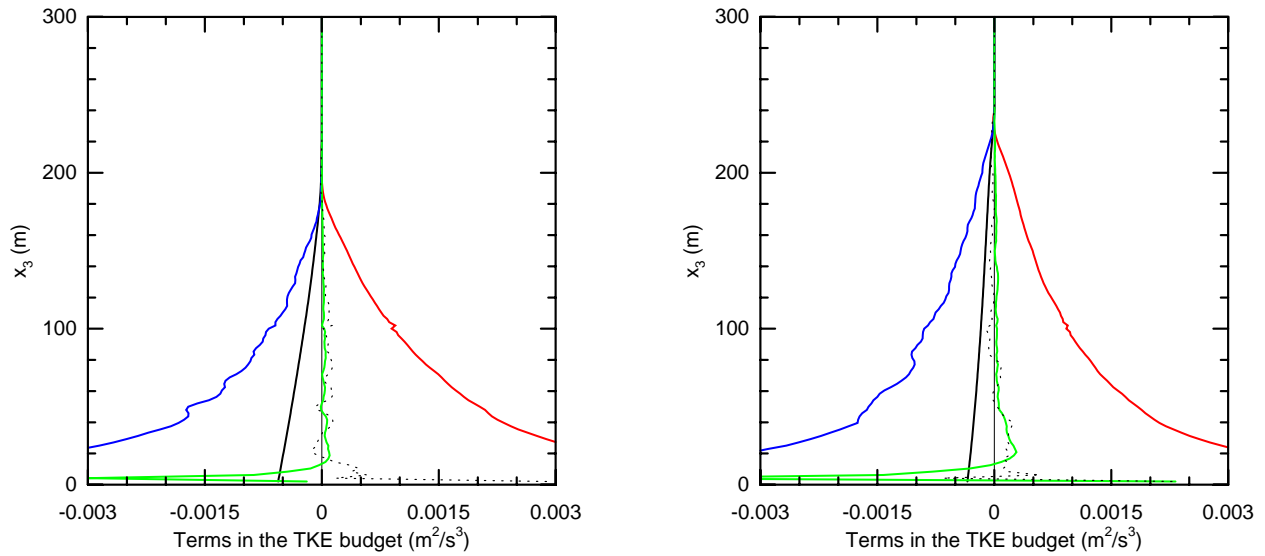


Figure 3: The TKE budget from simulations HOM (left panel) and HET (right panel). Red curves represent the effect of mean velocity shear, black – buoyancy, blue – dissipation, and green – the sum of third-order transport and pressure transport. Thin dotted black curves show the budget imbalance.

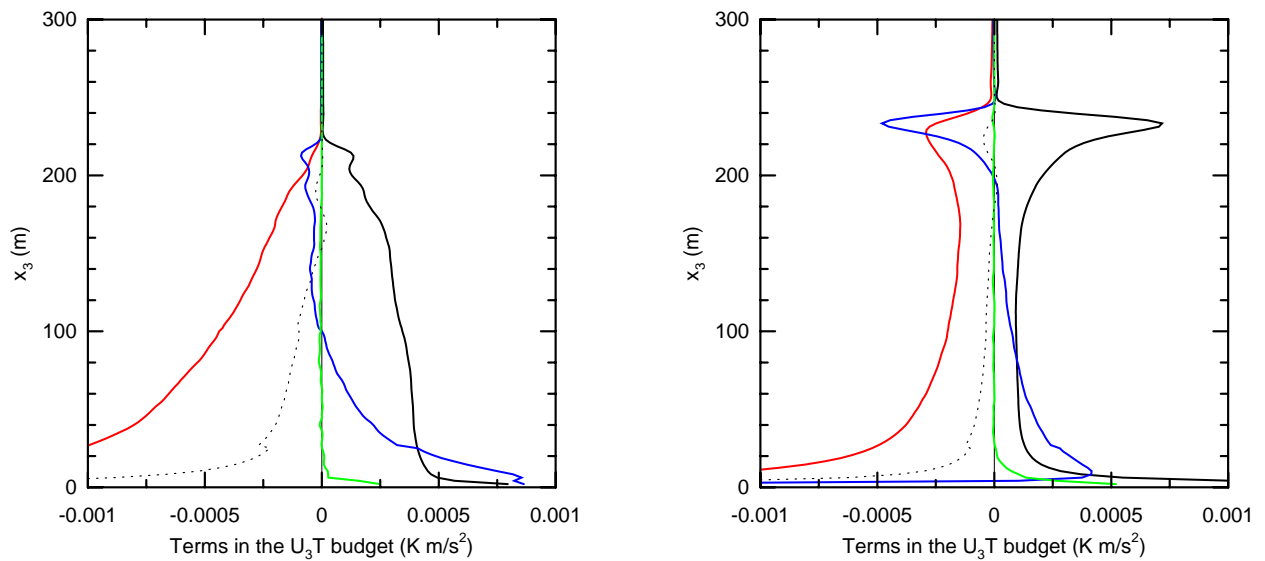


Figure 4: Budget of the vertical temperature flux from simulations HOM (left panel) and HET (right panel). Red curves represent the effect of mean temperature gradient, black – buoyancy, blue – pressure gradient-temperature covariance, and green – third-order transport. Thin dotted black curves show the budget imbalance.

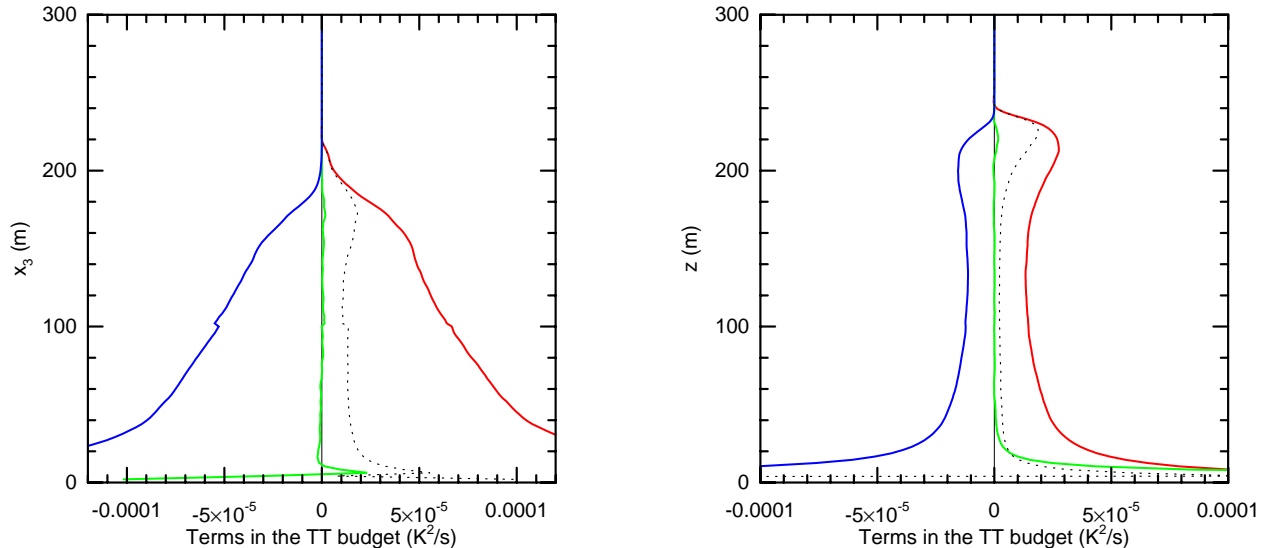


Figure 5: The temperature-variance budget from simulations HOM (left panel) and HET (right panel). Red curves represent the effect of mean temperature gradient, blue – dissipation, and green – third-order transport. Thin dotted black curves show the budget imbalance.

where several homogeneous parts with different surface temperatures are considered within a host model grid box and conventional surface-layer flux-profile relationships are applied to each part. This approach is being tested within the framework of a two-equation turbulence model, which carries transport equations for both the TKE and the temperature variance (E. Machulskaya, personal communication). Results will be reported later.

A word of caution about the fidelity of LES as applied to the SBL is in order. Since turbulence in the SBL is dominated by small-scale eddies and turbulent transport in most of the boundary layer essentially depends on the heat and momentum transfer near the surface, one may argue that LES of SBL is uncertain, except perhaps when the resolution is extremely high. The argument is valid and caution is indeed required when interpreting LES data on stably stratified flows. We believe, however, that our findings are grossly independent of possible LES uncertainties. For example, the third-order moment in the temperature-variance budget is large at the surface in the simulation HET and is identically zero in the simulation HOM. That is, we do not attempt to scrutinize a small difference of two large quantities, rather we compare quantities whose magnitudes are drastically different. Hence, the results should be qualitatively reliable, although the estimates of various turbulent quantities derived from LES may be somewhat uncertain in a quantitative sense.

One more issue related to the heterogeneous flows is the applicability of surface-layer flux-profile rela-

tionships in the LES. Sullivan et al. (1994) proposed an SGS model where the horizontal-mean momentum and temperature fluxes and the horizontal-mean profiles of velocity and temperature are forced to obey the Monin-Obukhov surface-layer similarity. As the Monin-Obukhov surface-layer flux-profile relationships are applicable to continuous turbulence over a homogeneous surface, it would be incorrect to enforce the Monin-Obukhov similarity in the horizontal-mean sense over a temperature-heterogeneous surface. We therefore apply the surface-layer relationships locally, i.e. point-by-point in the LES. On the other hand, the Monin-Obukhov similarity deals with the ensemble-mean quantities. Since turbulence near the surface is small-scale, a grid volume between the surface and the first model level above may contain a large enough ensemble of turbulent eddies which effectively makes a grid-volume mean a fair approximation to the ensemble mean. This is not a priori clear, however, so that some uncertainties remain. A possible way to improve the situation is to apply the surface-layer relationships to the quantities averaged over $n \times n$ grid points. The value of n should be chosen by trials, unless sound theoretical arguments can be adduced, so as to provide a good approximation to the ensemble-mean quantities, but it should still be small enough to avoid detectable surface heterogeneity within the area of $n \times n$ grid points. A detailed consideration of the surface-layer similarity as applied in LES of flows with heterogeneous underlying surface is beyond the scope of the present study (cf. Nakayama et al., 2004). It should be a sub-

ject for future work.

Note that our results are pertinent to the SBL with weak to moderate static stability. Although the cases HOM and HET are different in terms of the intensity of mixing, turbulence in both cases is well developed. In the future, a strongly stable boundary layer should be investigated, where turbulence over a homogeneous surface tends to die out. A key question is whether turbulence survives over a heterogeneous surface, and if so, whether it generates appreciable vertical fluxes of momentum and heat. The behavior of other turbulence statistics in strongly stable regime is also of considerable interest, e.g. if the surface flux of temperature variance remains positive. LES may not be an appropriate tool to study strongly stable regimes. DNS seems to be more appropriate, at least to obtain qualitative answers to the above questions.

One more important issue is the dependence of the SBL mean and turbulence structure on the size of the surface heterogeneity patterns. Stoll and Porté-Agel (2009) found that the magnitude of the temperature difference between the warm and the cold stripes has a pronounced effect on the SBL structure, whereas the results proved to be practically independent of the number of cold and warm stripes. Therefore, we chose the simplest configuration with one warm stripe and one cold stripe. Test runs with several warm and cold stripes (not shown) corroborate the finding of Stoll and Porté-Agel (2009). Recall that the flows in simulations of Stoll and Porté-Agel (2009) and in our simulations are in the weakly stable regime. Although the flows are stably stratified in a global (horizontal-mean) sense, vertical temperature gradient near the surface is negative in some regions of the flow. Due to the advection of cold air over warm surface, convective instability develops locally and convective vortices are formed. It is in this weakly stable regime that the results appear to be practically independent of the number of stripes (and hence of the size of the stripes relative to the domain size). In a strongly stable boundary layer, where the flow is statically stable (almost) everywhere, turbulence is likely to be strongly affected by internal gravity waves rather than vortices as in a weakly stable regime. Then, it cannot be stated a priori that the SBL structure would be grossly independent of the size of the surface heterogeneity patterns. Investigation of this issue should be a subject for future work.

6. CONCLUSIONS

Idealized LES of two SBL flows driven by fixed winds and homogeneous and heterogeneous surface temperature are compared. The LES data are used to compute statistical moments of the fluctuating fields (mean wind and mean potential temperature, second-order and

third-order turbulence moments, pressure-velocity and pressure-scalar covariances), to estimate terms in the second-moment budgets, and to assess the relative importance of various terms in maintaining the budgets. The budgets of TKE, temperature variance, and vertical temperature flux are analyzed. As different from most previous studies, the LES-based second-moment budgets are estimated with due regard for the sub-grid scale contributions. These contributions may be substantial, particularly in the SBL, and should be retained in order to close the second-moment budgets to a good order.

We find the SBL over a heterogeneous surface is more turbulent with larger TKE, is better mixed and is deeper compared to its homogeneous counterpart. Perhaps the most striking difference between the cases is exhibited by the temperature variance and its budget. Due to surface heterogeneity, the third-order moment, i.e. the vertical flux of temperature variance, is non-zero at the surface. Hence, the turbulent transport term (divergence of the above third-order moment) not only redistributes the temperature variance in the vertical, but is a net gain. An increase in the temperature variance near the surface helps explain a reduced magnitude of the downward temperature flux and more vigorous mixing in the heterogeneous case.

Motivated by the LES results, possible ways to incorporate the effect of the sub-grid scale surface temperature heterogeneity into the SBL turbulence models (parameterization schemes), including the surface-layer flux-profile relationships, are briefly discussed. One way is to use a tile approach where several parts with different surface temperatures are considered within a host model grid box.

Acknowledgments. We thank Vittorio Canuto, Sergey Danilov, Evgeni Fedorovich, Vladimir Gryanik, Donald Lenschow, Ekaterina Machulskaya, Chin-Hoh Moeng, Edward Patton, and Jeffrey Weil for useful discussions. The work was partially supported by the NCAR Geophysical Turbulence Program and by the European Commission through the COST Action ES0905.

REFERENCES

- Andrén, A., 1995: The structure of stably stratified atmospheric boundary layers. a large-eddy simulation study, *Quart. J. Roy. Meteorol. Soc.*, **121**, 961–985.
- Brown, A. R., S. H. Derbyshire, and P. J. Mason, 1994: Large-eddy simulation of stable atmospheric boundary layers with a revised stochastic subgrid model, *Quart. J. Roy. Meteorol. Soc.*, **120**, 1485–1512.

- Coleman, G. N., J. H. Ferziger, and P. R. Spalart, 1992: Direct simulation of the stably stratified turbulent Ekman layer, *J. Fluid Mech.*, **244**, 677–712.
- Deardorff, J. W., 1973: The use of subgrid transport equations in a three-dimensional model of atmospheric turbulence, *J. Fluids Engineering*, **95**, 429–438.
- Jiménez, M. A. and J. Cuxart, 2005: Large-eddy simulations of the stable boundary layer using the standard Kolmogorov theory: Range of applicability, *Boundary-Layer Meteorol.*, **115**, 241–261.
- Khanna, S., 1998: Comparison of Kansas data with high-resolution large-eddy simulation fields, *Boundary-Layer Meteorol.*, **88**, 121–144.
- Kosović, B. and J. A. Curry, 2000: A large eddy simulation study of a quasi-steady, stably stratified atmospheric boundary layer, *J. Atmos. Sci.*, **57**, 1052–1068.
- Lilly, D. K., 1967: The representation of small-scale turbulence in numerical simulation experiments, in *Proc. IBM Scientific Computing Symp. on Environmental Sciences*, edited by H. H. Goldstine, pp. 195–210, IBM Form No. 320-1951, Yorktown Heights, NY.
- Mason, P. J. and S. H. Derbyshire, 1990: Large-eddy simulation of the stably-stratified atmospheric boundary layer, *Boundary-Layer Meteorol.*, **53**, 117–162.
- Mironov, D. V., 2001: Pressure–potential-temperature covariance in convection with rotation, *Quart. J. Roy. Meteorol. Soc.*, **127**, 89–110.
- , 2009: Turbulence in the lower troposphere: second-order closure and mass-flux modelling frameworks, in *Interdisciplinary Aspects of Turbulence*, edited by W. Hillebrandt and F. Kupka, volume 756 of *Lect. Notes Phys.*, pp. 161–221, Springer-Verlag.
- Mironov, D. V., V. M. Gryanik, C.-H. Moeng, D. J. Olbers, and T. H. Warncke, 2000: Vertical turbulence structure and second-moment budgets in convection with rotation: a large-eddy simulation study, *Quart. J. Roy. Meteorol. Soc.*, **126**, 477–515.
- Moeng, C.-H., 1984: A large-eddy simulation model for the study of planetary boundary-layer turbulence, *J. Atmos. Sci.*, **41**, 2052–2062.
- Moeng, C. H. and J. C. Wyngaard, 1988: Spectral analysis of large-eddy simulations of the convective boundary layer, *J. Atmos. Sci.*, **45**, 3573–3587.
- Nakayama, A., H. Noda, and K. Maeda, 2004: Similarity of instantaneous and filtered velocity fields in the near wall region of zero-pressure gradient boundary layer, *Fluid Dynamics Research*, **35**, 299–321.
- Saiki, E. M., C.-H. Moeng, and P. P. Sullivan, 2000: Large-eddy simulation of the stably stratified planetary boundary layer, *Boundary-Layer Meteorol.*, **95**, 1–30.
- Stoll, R. and F. Porté-Agel, 2009: Surface heterogeneity effects on regional-scale fluxes in stable boundary layers: surface temperature transitions, *J. Atmos. Sci.*, **66**, 412–431.
- Sullivan, P. P., J. C. McWilliams, and C.-H. Moeng, 1994: A subgrid-scale model for large-eddy simulation of planetary boundary-layer flows, *Boundary-Layer Meteorol.*, **71**, 247–276.
- , 1996: A grid nesting method for large-eddy simulation of planetary boundary layer flows, *Boundary-Layer Meteorol.*, **80**, 167–202.
- Sullivan, P. P. and E. G. Patton, 2008: A highly parallel algorithm for turbulence simulations in planetary boundary layers: Results with meshes up to 1024^3 , in *18th Amer. Meteorol. Soc. Symp. on Boundary Layers and Turbulence*, Stockholm, Sweden, paper 11B.5, 11 pp.
- Taylor, J. R. and S. Sarkar, 2008: Stratification effects in a bottom Ekman layer, *J. Phys. Oceanogr.*, **38**, 2535–2555.
- van Dop, H. and S. Axelsen, 2007: Large eddy simulation of the stable boundary-layer: A retrospect to nieuwstadt’s early work, *Flow Turbul. Combust.*, **79**, 235–249.